Sustainable magnet-responsive nanomaterials for the removal of arsenic from contaminated water

Sustainable magnet-responsive nanomaterials for the removal of arsenic from contaminated water

Roberto Nisticò, Luisella Celi, Alessandra Bianco Prevot, Luciano Carlos, Giuliana Magnacca, Elena Zanzo, Maria Martin

Journal of Hazardous Materials
Volume 342, 15 January 2018, Pages 260-269

Sustainable magnet-responsive nanomaterials for the removal of arsenic from contaminated water

Roberto Nisticò[a,b,*], Luisella R. Celi[c], Alessandra Bianco Prevot[a], Luciano Carlos[d], Giuliana Magnacca[a,e], Elena Zanzo[c], Maria Martin[c]

[a] University of Torino, Department of Chemistry, Via P. Giuria 7, 10125 Torino, Italy.

[b] Polytechnic of Torino, Department of Applied Science and Technology DISAT, C.so Duca degli Abruzzi 24, 10129 Torino, Italy.

[c] University of Torino, Department of Agricultural, Forest and Food Sciences, Soil Biogeochemistry, Largo Paolo Braccini 2, 10095 Grugliasco, Italy.

[d] Instituto de Investigación y Desarrollo en Ingeniería de Procesos, Biotecnología y Energías Alternativas, PROBIEN (CONICET-UNCo), Buenos Aires 1400, Neuquén, Argentina.

[e] NIS (Nanostructured Interphases and Surfaces) Centre, Via P. Giuria 7, 10125 Torino, Italy.

*Corresponding author: E-mail: roberto.nistico@polito.it, Tel.: (+39)-011-0904745, Fax: (+39)-011-0904624

Abstract

In this study, chitosan and bio-based substances (BBS) obtained from composted biowaste were used as stabilizers for the synthesis of magnet-sensitive nanoparticles (NPs) via coprecipitation method. A pyrolysis treatment was carried out on both biopolymers at 550°C, and their consequent conversion into a carbon matrix was followed by means of different physicochemical characterization techniques (mainly FTIR spectroscopy and XRD), whereas magnetic properties were evaluated by magnetization curves. The prepared materials were tested in water remediation processes from arsenic (As) species (both inorganic and organic forms). These tests, explained by means of the most common adsorption models, evidenced that the best performances were reached by both materials obtained after pyrolysis treatments, pointing out the promising application of such magnet-sensitive materials as easy-recoverable tools for water purification treatments.

Keywords: Arsenic; Biomass valorization; Chitosan; Iron oxides; Magnetic materials; Pyrolysis.

1. Introduction

Arsenic (As) is the 20th most abundant element in the earth crust and is found in all environmental matrices (i.e., soil, water, air and in living matters) [1-2]. The most commonly available species of As in waters and soils are the inorganic forms: arsenite (containing As(III)) and arsenate (containing As(V)), together with the organic forms: monomethylarsonic acid (MMA) and dimethylarsinic acid (DMA) (**Scheme S1**) [2-3]. The International Agency for Research on Cancer (IARC) classified the As-containing compounds as group 1 carcinogen [4]. Since millions of people suffer from the arsenic poisoning as a result of the As-contaminated groundwater used as drinking water, for crop irrigation, and in food cooking [5], the removal of As from contaminated waters/soils, or its immobilization to avoid bioavailability, is one of the main relevant issues which caught the

attention of worldwide researchers. Rice (*Oryza sativa*) is the staple food for more than half of the world population, especially for the Asian countries. Previous investigations determined that rice is the primary food source of As exposure in non-seafood diets in EU [6].

In general, under oxidizing conditions (such as in aerobic soils and sediments) the predominant As form is arsenate, strongly bonded to soil Fe- and Al-containing minerals. After soil submersion, As occurs mainly as inorganic As(III) or in methylated organic forms (i.e., MMA and DMA). As(III) is more mobile and toxic than As(V), hence, in anoxic soils and aquifers As concentration in solution may dramatically increase following the reduction of As(V) to As(III) and the reductive dissolution of Fe oxy-hydroxides [7-10] on which As is retained.

The organic forms, DMA and MMA, even if considered less toxic than the inorganic ones, are readily mobilized at the solid-liquid interface, since they seem to become weakly bonded to the solid phases as the methyl-groups increase [11] and can be easily released in solution [12]. However, to date, the environmental behavior of the organic As form has been quite overlooked and scant information is available on removal options from waters and wastewaters [13].

As reported in the literature, conventional adsorbents used for the removal of As-species are activated carbons, oxides, and resins with poor adsorption capacity, which require a difficult separation step ([14-15] and references within). Due to the strong interaction between Fe and As, it appears very convenient to use easily-recoverable magnet-sensitive iron oxides as sequestrating agents for the removal of As species from contaminated soils and waters [16-20]. In this context, innovative water and wastewater treatments have been reported, involving the use of magnetic iron-based nanoparticles (NPs) stabilized by low-cost bio-based sources (i.e. biomasses and humic/fulvic acids, chitosan and its derivatives, polysaccharides, etc…) as novel adsorbents/active species for the removal of pollutants, thus guaranteeing both economic and environmental benefits [21-28].

The most common magnetic iron-based material is magnetite ($FeO•Fe_2O_3$) which is sensitive to oxidation forming maghemite (γ-Fe_2O_3) and successively the non-magnetic phase hematite (α-

Fe_2O_3) [29]. In order to avoid the complete oxidation and the lack of the magnetic properties, the magnetic particles need to be stabilized by a protective layer [30-31]. Quite recently, we investigated the feasibility of low-cost biopolymers obtained from natural sources as stabilizing coatings for magnetite/maghemite production via coprecipitation reaction [30-33]. In this context, bio-based substances obtained from green compost (BBS-GC, **Table S1** [34]), i.e., lignin-derived macromolecules with a humic-like structure, are good stabilizers for the production of BBS-covered magnetic NPs [31]. On the other hand, chitosan is an aminopolysaccharide derived from chitin, one of the most abundant natural biopolymers forming the crustaceous and insect exoskeleton and the cell walls of some fungi [35-37]. Chitosan, thanks to its freely available and reactive amino groups can be used in several applications, such as drug carrier in biomedicine [38-39] as well as green adsorbent for the removal of pollutants from contaminated water [22,40]. In addition, chitosan can also encapsulate magnet-sensitive iron oxide NPs [30,33,41-42]. Lastly, both substrates (i.e., BBS-GC and chitosan), when used to prepare coated hybrid magnetic NPs, can be easily converted into a carbon coating through pyrolysis at 550°C maintaining the magnetic behaviors [32,33,43].

Based on these considerations we hypothesize that these nanomaterials may be used as adsorbents for As removal and that their efficiency is a function of their surface properties and affinity towards the different As forms. To test these hypotheses we evaluated the removal efficiency of inorganic As(V), As(III) and organic DMA from contaminated waters by means of magnet-sensitive NPs stabilized by green and sustainable materials, namely BBS, chitosan and their carbon-derived forms. In view of the practical application of these substrates, we studied As adsorption/desorption with the aim of discriminating between the formation of inner- and outer-sphere complexes, which affect the reversibility of As bonding, and then the effective sequestration of the contaminant from the solution.

2. Experimental

2.1 Materials

Precursors selected for the magnetite synthesis were anhydrous ferric chloride $FeCl_3$ (CAS 7705-08-0, purity ≥ 98.0%, Fluka) and ferrous sulphate heptahydrate $FeSO_4 \cdot 7H_2O$ (CAS 7782-63-0, purity ≥ 99.5%, Fluka). Bio-Based Substances (BBS-GC) isolated from composted urban biowastes (i.e., urban public park trimming and home gardening residues) were obtained from the *ACEA Pinerolese Industriale S.p.A.* waste treatment plant located in Pinerolo (Italy). Medium molecular weight chitosan obtained from crab shells (DD = 75–85%) was purchased from Aldrich. Arsenic sources were: sodium arsenate dibasic heptahydrate ($Na_2HAsO_4 \cdot 7H_2O$, CAS 10048-95-0, essay ≥ 98.0%, Sigma), sodium (meta)arsenite ($NaAsO_2$, CAS 7784-46-5, essay ≥ 90.0, Aldrich), and dimethylarsinic acid (DMA, $C_2H_7AsO_2$, CAS 75-60-5, essay ≥ 98.0%, Sigma). Other reagents used were: ammonium hydroxide solution (CAS 1336-21-6, NH_3 essay 28-30%, E. Merck), sodium hydroxide (NaOH, purity ≥ 98.0%, CAS 1310-73-2, Sigma-Aldrich), hydrochloric acid (HCl, conc. 37 wt.%, CAS 7647-01-0, Fluka), anhydrous potassium chloride (KCl, CAS 7447-40-7, purity ≥ 99.0%, Fluka), and anhydrous potassium phosphate monobasic (KH_2PO_4, purity ≥ 99%, CAS 7778-77-0, Sigma-Aldrich). All aqueous solutions were prepared using ultrapure water Millipore Milli-Q™. All chemicals were used without further purification.

2.2 Preparation of the stabilized magnetic NPs

Magnetic nanoparticles were prepared following a procedure already reported in the literature [31,33]. In detail, 3.7 g of $FeCl_3$ and 4.17 g of $FeSO_4 \cdot 7H_2O$ (molar ratio Fe(III)/Fe(II) = 1.5) were dissolved in 100 mL of deionized water and heated up to 90°C. At this target temperature, two solutions were added simultaneously: a) 10 mL of 28-30% ammonium hydroxide, and b) 50 mL of the aqueous solution containing the stabilizers, either 1 wt.% BBS solution or 1 wt.% chitosan in

weak acid environment (2 vol.% HCl, mandatory to reach the complete chitosan dissolution). The final black mixture was mechanically stirred at 90°C for 30 min and then cooled down to room temperature (RT). The obtained precipitates (either BBS-stabilized or chitosan-stabilized magnetic materials) were then purified by washing several times with deionized water and oven-dried at 80°C overnight. Part of the obtained materials was thermally treated in a quartz tube reactor at 550°C (heating rate of 5°C min^{-1}) under nitrogen atmosphere (N_2 flow: 250 mL min^{-1}) for 1 hour. Depending on both composition and thermal treatment, magnet-sensitive materials were coded as follows: MB0 (BBS-stabilized magnetic material), MC0 (chitosan-stabilized magnetic material), MBP (BBS-stabilized material after pyrolysis at 550°C, still magnetic), and MCP (chitosan-stabilized material after pyrolysis at 550°C, still magnetic). The obtained materials have been stored dried at room temperature before use: in these conditions they show long-term stability.

Non-stabilized magnetic material (M0) was obtained as well without addition of any stabilizers and without pyrolysis treatment, as control.

2.3 Physicochemical characterization

X-ray diffraction (XRD) patterns were obtained by means of an X'Pert PRO MPD diffractometer from PANalytical, equipped with Cu anode, working at 45 kV and 40 mA, in a Bragg-Brentano geometry performing experiments on flat sample-holder configurations. The acquisition was performed in a 0.02° interval steps, with 45 s $step^{-1}$ to obtain a good signal to noise ratio. Fourier transform infrared (FTIR) spectra were recorded in transmission mode (Bruker Vector 22 spectrophotometer equipped with Globar source, DTGS detector), acquiring 128 scans at 4 cm^{-1} resolution in the 4000-400 cm^{-1} range. Samples were mixed with KBr (1:20 weight ratio). Magnetization measurements were carried out with a LakeShore 7404 vibrating sample magnetometer. The hysteresis loop of the samples was registered at RT and the magnetic field was cycled between -20000 and 20000 Oersted.

2.4 Removal of arsenic species from contaminated waters: adsorption experiments

Adsorption experiments were performed in triplicate in closed test tubes by dispersing 20 mg of magnet-sensitive materials in 5 mL of 0.01M KCl solution and adding HCl or NaOH to reach a final pH value of 6.0 ± 0.5. This value is suitable for all the considered As species and it is commonly found in natural environments; moreover it guarantees the stability of the materials, since chitosan and magnetite can be solubilised in acid environment, whereas the hybrid BBS-magnetite system is not stable in basic environment.

Preliminary adsorption experiments carried out with different contact times demonstrated that most of the adsorption process occurred within the first few hours. A precautionary contact time of 24h was chosen to guarantee that the adsorption process was completed before performing the desorption experiments.

Arsenic-containing species were then prepared in the 50-500 mg As L^{-1} range in 0.01M KCl at pH 6.0 and added to the suspensions to reach the desired concentration (C_0 = 5, 10, 20, 30, 50, 60, 120, 240, 300 mg L^{-1} of As). The suspensions were shaken for 24 h on a reciprocal shaker at 60 rpm in a climatic chamber in the dark at 25°C. After shaking, sorbents were magnetically separated from the solution, and solutions filtered through 0.2 μm filter membrane. The As concentration in the sampled solution (Ce, mg L^{-1}) was determined by Hydride Generation-Atomic Absorption Spectroscopy HG-AAS (Perkin-Elmer 4100 equipped with a FIAS 400 hydride generator; Perkin-Elmer Inc., Waltham, Massachusetts), whereas the amount of sorbed As (qe, mg g^{-1}) was calculated as follows (**Equation 1**):

$$qe = [V(C_0\text{-}Ce)]/m \quad (\mathbf{1})$$

where C_0 is the initial arsenic concentration in the solution (mg L^{-1}), Ce is the equilibrium concentration of free arsenic species in the solution measured by HG-AAS (mg L^{-1}), V is the solution volume (10 mL) and m is the mass of the magnet-sensitive materials (20 mg). The sorbed As amount was reported on weight/weight basis and not as a function of the specific surface area of the sorbing materials since the measured surface area of the solid carried out by N_2 adsorption at 77 K (below 10 m^2 g^{-1}) corresponds to aggregated powders and does not reflect the actual exposed surface in the sorbent aqueous suspension. In fact the diameter of the primary particles as determined by TEM analysis is about 10 nm, value corresponding to much higher specific surface area.

All experiments were duplicated. The experimental error, estimated by **Equation 2** [44] was lower than 5%.

$$\Delta qe/qe = \Delta Ce/(C_0\text{-}Ce) \qquad (2)$$

2.5 Removal of arsenic species from contaminated water: desorption experiments

To evaluate the reversibility of the adsorption of the different As species on the materials, desorption experiments were performed for each separate batch by adding the extracting media directly to the wet As-containing magnet-sensitive materials previously magnetically-separated from the solution. In detail, the wet As-containing magnet-sensitive materials (for desorption tests only thermally-treated substrates were considered, i.e. MCP and MBP) were dispersed in 0.01M KCl at pH = 6.0. This washing step was introduced to eliminate the residual As-spiked solution used for the saturation of the adsorbent, and to determine the weakly bound As. The pH of the suspensions was further corrected to reach the final pH value of 6.0 ± 0.5. The suspensions were shaken for 24 h on a reciprocal shaker at 60 rpm in a climatic chamber in the dark at 25°C. Sorbents were then magnetically separated from the solution, and solutions filtered through 0.2 μm filter

membrane. The residues were then treated with 0.1M KH_2PO_4 (chosen since phosphate groups can selectively substitute As) at pH 6.0 and the procedure repeated as described above, to determine the phosphate-exchangeable As fraction.

2.6 Isotherms modeling

In order to rationalize the isothermal trends, both Langmuir [45] and Freundlich [46] adsorption models were selected. The Langmuir model [45] refers mainly to adsorption isotherms that present a saturation phenomenon. In fact, in the Langmuir model the qe value (i.e., mass of sorbed solute per unit mass of sorbent) increases linearly at low surface coverage, reaching an asymptotic trend approaching the saturation. This model is based on the assumptions that the adsorption is limited to the monolayer, with the same sorption energy for all adsorbing sites, independently from the surface coverage, and excluding the interactions among adjacent sites [45,47].

The Freundlich model [46] is an empirical equation that refers mainly to multilayer adsorption. Basically, this model relies on adsorbents with heterogeneous surface with several adsorption sites.

3. Results and Discussion

3.1 Physicochemical and magnetic characterization

X-ray diffraction (XRD) analysis was used to identify the iron oxide phase present in all samples (**Figure 1**, panels **A** and **B**). All the main signals highlighted (orange boxes) in both figures at 2θ = 30.1° (220), 35.4° (311), 43.0° (400), 53.9° (422) 57.2° (511), and 62.6° (440) are consistent with the presence of magnetite/maghemite phase (card numbers 00-019-0629 and 00-039-1346, ICCD Database) [31]. No relevant reflections are expected from both BBS and chitosan since their XRD pattern presents only few negligible signals [26,33]. In samples MC0, MCP and MBP extra signals not related to the expected phase (the main relevant one registered at 2θ = 33°) are due to the presence of ammonium-containing salts: i.e., ammonium chloride (card number 01-073-0363,

ICCD Database) obtained as byproducts of the co-precipitation reaction. The presence of such byproducts is related to the washing step, and consequently to the sample cleanness. Thermally treated materials (namely MCP and MBP) still present the main reflections due to magnetite.

Infrared spectra of all magnet-sensitive samples and reference materials (bare magnetite/maghemite, chitosan and BBS) are shown in **Figure 1 (**panels **C** and **D**). MC0 infrared signals at 1655 cm^{-1} (due to axial C=O stretching mode, amide I), at 1580 cm^{-1} (due to angular N-H deformation mode, amide II) and the broad signal in the 1150-900 cm^{-1} range (due to the glycosidic ring C-O and C-O-C stretching mode) confirm the presence of chitosan (**Figure 1C**, blue boxes), whereas the signals in the 575-620 cm^{-1} range (due to Fe-O stretching vibrations) confirm the iron oxide phase (**Figure 1C**, violet box) [33]. Additionally, a sharp and pointed peak at ca. 1400 cm^{-1} (**Figure 1C**, red box) evidenced the carboxylate-induced interactions [48-49]. Pyrolysis thermal treatment at 550°C evidenced the disappearance in MCP profile of all chitosan principal signals with formation of a very sharp band at ca. 1600 cm^{-1} typical of graphite-like C=C stretching mode (attributed to the formation of a carbon phase). Infrared signals in the 575-620 cm^{-1} range due to Fe-O stretching mode are still maintained (**Figure 1C**, violet box). Analogously, in MB0 infrared spectrum the signals at ca. 1600 cm^{-1} (due to carboxylate stretching mode) and at 1120 cm^{-1} (due to C-O stretching mode) are associated with the presence of BBS (**Figure 1D**, green boxes), whereas the sharp peak at ca. 1400 cm^{-1} confirmed the carboxylate-induced interactions (**Figure 1D**, red box) [50]. Magnetite/maghemite phase is clearly supported by the presence of magnetite Fe-O signals (**Figure 1D**, violet box). Analogously to MCP, even MBP evidenced the disappearance of the signals corresponding to the organic BBS component, with formation of the C=C infrared peak at ca. 1600 cm^{-1} due to the conversion of BBS into a carbon structure still maintaining the magnetite/maghemite phase (**Figure 1D**, violet box).

Magnetic properties of such materials were evaluated by means of magnetization curves collected at RT (magnetization curves profiles are reported in **Figure 1**, panels **E** and **F**, whereas numerical

values are summarized in **Table S2**). As suggested by the very narrow hysteresis loop, all samples clearly revealed a superparamagnetic behavior [42,51]. Bare materials (i.e., M0, MB0, and MC0) have both low remanence (residual magnetism, M_r = 0.1-1.1 emu g^{-1}), and intrinsic coercitivity (the field necessary to bring the magnetization to zero, H_{ic} below 10 Oe), with saturation magnetization values of 64 emu g^{-1} (M0), 53 emu g^{-1} (MB0), and 39 emu g^{-1} (MC0), respectively. In general, the difference in terms of saturation magnetization with respect to the reference magnetite/maghemite M0 is mostly due to the presence of not-magnet-sensitive organic coatings surrounding the magnetic NPs, which cause quenching of the surface magnetic moments [42,52-53]. As already evidenced in our previous works [33], materials produced after pyrolysis treatment (namely, MBP and MCP) affect both the remanence (M_r increases to ca. 5 emu g^{-1}) and mainly the instrinsic coercitivity (H_{ic} moves to values higher than 80 Oe), whereas magnetization saturations slightly decrease to 45 emu g^{-1} (MBP), and 30 emu g^{-1} (MCP).

Basing on the results shown in ref. [23, 33], both MC0 and MCP samples are in form of microagglomerates in the 0.5-5.0 μm range, showing an irregular and complex surface. Similar results were also obtained for MB0 and MBP samples, with formation of agglomerates in the 20-50 nm range.

3.2 Adsorption/desorption of As(V) and As(III)

Adsorption experiments were performed in order to evaluate the potential application of such magnet-sensitive materials for the removal of inorganic arsenic species from contaminated waters.

The curve profiles reported in **Figure 2** evidenced that best adsorption performances were obtained by thermally-treated materials (i.e., carbon-coated NPs) with As(V), as both MCP and MBP were able to adsorb up to 101 and 53 mg As g^{-1}, respectively. Lower amounts of As (III) were retained with the best performances again with the thermally-treated sorbents, clearly highlighting that these systems are more efficient in adsorbing As than the untreated ones. At the same experimental

conditions (i.e., RT and circumneutral pH), chitosan gave an adsorption capacity for As(V) of 0.73 mg g^{-1}, biochar (from rice husk) 7.1 mg g^{-1}, while Fe-coated biochar gave 15.2 mg g^{-1}, whereas magnetite-based systems reached the value of 204 mg g^{-1} at basic pH (pH 8) [54]. Concerning As(III), magnetite NPs obtained from tea waste evidenced, at neutral pH and at 30°C, an adsorption capacity of 189 mg g^{-1} [54-55]. Interestingly, the material shape was also important since iron-chitosan flakes (at pH 7 and 25°C) adsorb 16.2 mg g^{-1} of As(III) and 22.5 mg g^{-1} of As(V), whereas by using iron-chitosan granules, the adsorption performances decreased to values in the 2.2-2.3 mg g^{-1} range [54,56]. These data evidenced that the MCP performance is extremely promising and encouraging, in particular towards As(V) sequestration, coupling a good adsorption capacity with the practical advantages of a nanosized but easily recoverable magnetic substrate.

The performances of the magnetite-based adsorbents on As(III) adsorption could even improve by increasing the pH [57], considering the dissociation constants of the arsenous acid (pKa_1=9.2). However, at the same time, arsenate adsorption would be negatively affected [57-58] and drop at pH higher than the PZC of the materials [23].

To rationalize the adsorption behaviors of both MCP and MBP against the three As forms investigated, both Langmuir and Freundlich adsorption equations have been applied (**Figure S1)** and the estimated parameters and constants obtained from the two models are summarized in **Table 1**. The determination coefficient R^2 (**Table 1**) suggested that the Langmuir equation better predict the sorption isotherm profiles for As(III) on both the investigated substrates (i.e., MCP and MBP), whereas the Freundlich model better fits the sorption profiles for As(V). The Langmuir equation often provides good fits for anion adsorption on metal oxides, when the adsorbing sites are relatively homogeneous and an adsorption plateau (theoretically a monolayer) is asymptotically reached [59], although this does not allow to infer mechanistic explanations for ion adsorption in aqueous solution, since the theoretical assumptions of the model are not fully satisfied in such systems [60]. However, Langmuir parameters (q_0, the adsorption maximum, and b, a constant

related to the adsorbent-adsorbate affinity) can be of practical use for comparisons among adsorbing substrates and adsorbed species. In the present case, Langmuir parameters would suggest that As(V) is retained on both MCP and MBP not only in much greater amounts than As(III), but also with higher affinity. Hence, MCP would be the best choice for As(V) adsorption considering both retained amount and adsorption affinity. Conversely, the two adsorbents perform substantially equally for As(III) adsorption. However these considerations, although practically useful, should be taken as merely indicative, particularly if considering that for As(V) adsorption, the fitting to Freudlich equation improved slightly compared with Langmuir one. This commonly happens when the adsorption occurs on heterogeneous sites and does not reach a plateau, that seems the case of As(V) adsorption on both substrates [58]. This means that, in the tested concentration range, the surfaces are not yet approaching the saturation and As sequestration on the solid phase is still increasing even at the highest As additions. Additionally, all sorption phenomena are favorable under the present experimental conditions, since the Freundlich exponent n is always in the 1-10 range and values of $1/n<1$, here occurring for all the adsorbent/adsorbate couples, are often interpreted as indicative of chemisorption [59].

The desorption experiments performed on the thermally-treated samples (i.e., MCP and MBP) clearly show that at the selected conditions the As(V) inorganic form was almost not released in the presence of 0.01M KCl and less than 20% with 0.1M KH_2PO_4 (**Figure 3**), highlighting that the adsorption reaction is mainly irreversible for both magnet-sensitive materials (residual As(V) $\geq$ 80%). Conversely, since As(III) is weakly adsorbed by both substrates, in agreement with the lower values of Langmuir b parameter (**Table 1**), the desorption is more effective, in particular for MBP (residual As(III) ca. = 48%).

A limited number of publications reports desorption experiments from magnetite-based adsorbents (see [61] and references therein), however, a scarce reversibility of the adsorption process could be expected for both As(V) and As(III) [62]. This can be attributed to the specific mechanisms

dominating As adsorption on Fe (hydr)oxide surfaces, mainly involving the formation of inner-sphere complexes through ligand exchange (e.g., [63] and references therein). In particular, on magnetite, As(V) adsorbs with a bidentate, binuclear, corner-sharing complex [57], while for As(III), besides bidentate complexes [57], also the formation of tridentate, hexanuclear, corner-sharing complexes has been proposed [64-65]. The well assessed inner-sphere adsorption mechanisms of As species on magnetite are not likely to be modified for the tested substrates by the stabilization procedure here used to ensure the long term stability of magnetite. The presence of an organically-derived component in the tested adsorbents did not diminish, indeed, the high stability of the As-magnetite complexes, as confirmed by the results of the competitive desorption experiments, strongly suggesting that the inner-sphere complexes forming between As and the metal surfaces, evidenced for pure magnetite, dominate As adsorption also with these stabilized materials. The slightly greater desorbability of As(III) compared with As(V) supports the formation of more labile bindings to the adsorbent surface and a though limited presence of outer-sphere complexes cannot thus be ruled out.

The strong As retention on the adsorbent surfaces, on one side, would limit the possibility of regeneration and reuse of the spent adsorbent, also considering that the application of strongly alkaline regenerants (such as NaOH), commonly used for this purpose [61] would involve a partial dissolution of the substrate. On the other side, the scarce risk of As leaching would facilitate the management and storage of the spent adsorbents.

3.3 Adsorption/desorption of DMA

In submerged soils and sediments organic forms, mainly represented by dimethylarsinic acid (DMA) [66], often occur besides the inorganic ones [67-70] and, although generally less represented, these forms are difficult to be removed by adsorption, particularly DMA [11]. Hence, the possible use of thermally-treated magnet-sensitive materials in the removal of DMA from contaminated water was also evaluated. Isothermal adsorption on MCP and MBP substrates at the

same conditions of inorganic forms are reported in **Figure 4**. The best DMA adsorption performances are obtained with MBP, with a Langmuir adsorption maximum of 17.2 mg g^{-1} of DMA (**Table 1**). This result, obtained at pH 6, commonly found in natural environments, is encouraging, since DMA is known to be adsorbed more at acidic than at circumneutral pH [12]. Similar performances have been reported at circumneutral pH with Zr-modified membranes [68], which gave better results only at very acidic pH. The adsorption capacity of MCP vs. DMA was significantly lower (i.e., a Langmuir q_0 of 9.0 mg g^{-1}), although it was still higher than that reported for other chitosan-based adsorbents, even at lower pH [71].

Comparing these results with the experiments carried out on inorganic forms (see **Figure S1**), both substrates show a different affinity toward the arsenic forms following the order: As(V) > As(III) ≥ DMA, similarly to untreated Fe oxides [12] and Al oxides [72], confirming that, also with these adsorbents, As methylation results in decreased adsorbed amounts.

Desorption experiments performed directly on the DMA-saturated sorbents (**Figure 5**) evidenced that at the selected conditions the organic form DMA is strongly bonded to both substrates (residual DMA ≥ 80%), similarly to As(V), and even phosphate was not able to displace DMA from adsorbing sites. The strong interaction between DMA and the adsorbents could be explained by recent reports suggesting the formation of inner-sphere, bidentate, binuclear complexes on soil Fe-compounds even for DMA, and not only for MMA, although some outer-sphere complexes may also be formed [69-70]. However, considering the large percentage of DMA desorbed by phosphate from other pure Fe oxides [12,73] as well as from Al oxides [72], this result was quite unexpected, and could suggest a dominance of inner-sphere interaction in the case of MCP and MBP substrates. The latter adsorbent, in particular, although less effective in the sequestration of inorganic As, can retain the largest amounts of DMA almost irreversibly. This may be encouraging in view of the effective sequestration of this As form, although posing limitations to the regeneration of the spent adsorbent.

4. Conclusions

Biopolymers, such as chitosan and lignin-derived bio-based substances extracted from composted biowaste, were used as stabilizers for magnetic iron oxide NPs production via coprecipitation method. The effect of pyrolysis treatment at 550°C, and the consequent conversion of both biopolymers into a carbon matrix, was followed by means of several physicochemical characterization techniques (i.e., mainly FTIR and XRD), whereas magnetic properties were evaluated by magnetization curves.

Such easily-recoverable materials, just applying an external magnetic field, were tested in water remediation processes from As species. The results evidenced that the best performances were reached by both materials obtained after pyrolysis (i.e., magnetite/carbon NPs), with different adsorption capacity and reversibility, as a function of the As species. Adsorption extent and its generally scarce reversibility suggest a higher retention capacity when As is dissolved in water in form of As(V), although all the tested As species were adsorbed on the pyrolyzed materials. These substrates showed particularly good performances in strongly bonding DMA, which is generally scarcely retained by Fe and Al oxides.

The high efficiency of As removal, compared to literature data, along with the magnetic properties showed by these materials, clearly demonstrate that these iron oxide systems can be successfully used as a green, sustainable, versatile and low cost adsorbent for the remediation of waters contaminated by As(V) and As(III) species, including organic forms.

5. Acknowledgements

This work was realized with the financial support for academic interchange by the Marie Sklodowska-Curie Research and Innovation Staff Exchange project funded by the European Commission H2020-MSCA-RISE-2014 within the framework of the research project Mat4treaT

(Project number: 645551). Compagnia di San Paolo and University of Torino are gratefully acknowledged for funding Project Torino_call2014_L2_126 through ‘‘Bando per il finanziamento di progetti di ricerca di Ateneo – anno 2014’’ (Project acronym: Microbusters). Additionally, authors would like to acknowledge Dr. Flavio R. Sives (Universidad Nacional de La Plata, Argentina) for performing the magnetization measurements, together with Marco Prati and Cristina Lerda (University of Torino, Italy) for their precious help.

References

[1] M. Azizur Rahman, H. Hasegawa, High levels of inorganic arsenic in rice in areas where arsenic-contaminated water is used for irrigation and cooking, **Science of the Total Environment** 409 (2011) 4645-4655.

[2] A. Sommella, C. Deacon, G. Norton, M. Pigna, A. Violante, A.A. Meharg, Total arsenic, inorganic arsenic, and other elements concentrations in Italian rice grain varies with origin and type, **Environmental Pollution** 181 (2013) 38-43.

[3] E. Smith, R. Naidu, A.M. Alston, Arsenic in the soil environment, **Advances Agronomy** 64 (1998) 149-195.

[4] IARC (International Agency for Cancer Research), *Some Drinking-water Disinfectants and Contaminants, Including Arsenic*, 84, IARC, Geneva, Switzerland (2004).

[5] A.A. Carbonell-Barrachina, A.J. Signes-Pastor, L. Vazquez-Araffljo, F. Burlo, B. Sengupta, resence of arsenic in agricultural products from arsenic-endemic areas and strategies to reduce arsenic intake in rural villages, **Molecular Nutrition Food Research** 53 (2009) 531-541.

[6] H. Robberecht, R. Van Cauwenbergh, D. Bosscher, R. Cornelis, H. Deelstra, Daily dietary total arsenic intake in Belgium using duplicate portion sampling and elemental content of various foodstuffs, **European Food Research and Technology** 214 (2002) 27-32.

[7] P.L Smedley, D.G Kinniburgh, A review of the source, behaviour and distribution of arsenic in natural waters, **Applied Geochemistry** 17 (2002) 517–568.

[8] M. Martin, R. Ferdousi, K.M.J. Hossain, E. Barberis, Arsenic from groundwater to paddy fields in Bangladesh: Solid-liquid partition, sorption and mobility, **Water, Air, and Soil Pollution** 212 (2010) 27-36.

[9] M. Martin, A. Violante, F. Ajmone-Marsan, E. Barberis, Surface interactions of arsenite and arsenate on soil colloids, **Soil Science Society of America Journal** 78 (2014) 157-170.

[10] S. Dixit, J.G. Hering, Comparison of arsenic(V) and arsenic(III) sorption onto iron oxide minerals: Implications for arsenic mobility, **Environmental Science & Technology** 37 (2003) 4182-4189.

[11] J.S. Zhang, R.S. Stanforth, S.O. Pehkonen. Effect of replacing a hydroxyl group with a methyl group on arsenic(V) species adsorption on goethite (α-FeOOH), **Journal of Colloid and Interface Science** 306 (2007) 16–21.

[12] B.J. Lafferty, R.H. Loeppert, Methyl arsenic adsorption and desorption behavior on iron oxides, **Environmental Science and Technology** 39 (2005) 2120-2127.

[13] Z. Cheng, A. van Geen, R. Louis, N. Nikolaidis, R. Bailey. Removal of methylated arsenic from groundwater with iron filings, **Environmental Science and Technology** 39 (2005) 7662–7666.

[14] T. Tuutijärvi, J. Lu, M. Sillanpää, G. Chen, As(V) adsorption on maghemite nanoparticles, **Journal of Hazardous Materials** 166 (2009) 1415–1420.

[15] D. Mohan, C.U. Pittman Jr., Arsenic removal from water/wastewater using adsorbents—A critical review, **Journal of Hazardous Materials** 142 (2007) 1-53.

[16] Z. Bujňáková, P. Baláž, A. Zorkovská, M.J. Sayagués, J. Kováč, M. Timko, Arsenic sorption by nanocrystalline magnetite: An example of environmentally promising interface with geosphere, **Journal of Hazardous Materials** 262 (2013) 1204-1212.

[17] Y. Yoon, W.K. Park, T.-M. Hwang, D.H. Yoon, W.S. Yang, J.-W. Kanga, Comparative evaluation of magnetite-graphene oxide and magnetite-reduced graphene oxide composite for As(III) and As(V) removal, **Journal of Hazardous Materials** 304 (2016) 196-204.

[18] Y. Mamindy-Pajany, C. Hurel, N. Marmier, M. Roméo, Arsenic (V) adsorption from aqueous solution onto goethite, hematite, magnetite and zero-valent iron: Effects of pH, concentration and reversibility, **Desalination** 281 (2011) 93–99.

[19] Y.-F. Lin, J.-L. Chen, C.-Y. Xu, T.-W. Chung, One-pot synthesis of paramagnetic iron(III) hydroxide nanoplates and ferrimagnetic magnetite nanoparticles for the removal of arsenic ions, **Chemical Engineering Journal** 250 (2014) 409–415.

[20] B. Casentini, F.T. Falcione, S. Amalfitano, S. Fazi, S. Rossetti, Arsenic removal by discontinuous ZVI two steps system for drinking water production at household scale, **Water Research** 106 (2016) 135–145.

[21] G. Magnacca, E. Laurenti, M.C. González, A. Arques, A. Bianco Prevot, *Effect of humic substances and bioorganic substrates from urban wastes in nanostructured materials applications and synthesis*, In: A. Arques, A. Bianco Prevot (Eds.), Soluble Bio-based Substances Isolated from Urban Wastes. Environmental Applications, Springer International Publishing AG, Cham (Switzerland), 2015, pp. 41-58.

[22] W.S. Wan Ngah, L.C. Teong, M.A.K.M. Hanafiah, Adsorption of dyes and heavy metal ions by chitosan composites: A review, **Carbohydrate Polymers** 83 (2011) 1446-1456.

[23] G. Magnacca, A. Allera, E. Montoneri, L. Celi, D.E. Benito, L.G. Gagliardi, M.C. González, D.O. Mártire, L. Carlos, Novel magnetite nanoparticles coated with waste-sourced biobased substances as sustainable and renewable adsorbing materials, **ACS Sustainable Chemistry and Engineering** 2 (2014) 1518-1524.

[24] J. Gomis, R.F. Vercher, A.M. Amat, D.O. Mártire, M.C. González, A. Bianco Prevot, E. Montoneri, A. Arques, L. Carlos, Application of soluble bio-organic substances (SBO) as

photocatalysts for wastewater treatment: Sensitizing effect and photo-Fenton-like process, **Catalysis Today**209 (2013) 176-180.

[25] J. Gomis, L. Carlos, A. Bianco Prevot, A.C.S.C. Teixeira, M. Mora, A.M. Amat, R. Vicente, A. Arques, Bio-based substances from urban waste as auxiliaries for solar photo-Fenton treatment under mild conditions: Optimization of operational variables, **Catalysis Today** 240A (2015) 39-45.

[26] A. Bianco Prevot, F. Baino, D. Fabbri, F. Franzoso, G. Magnacca, R. Nisticò, A. Arques, Urban biowaste-derived sensitizing materials for caffeine photodegradation, **Environmental Science and Pollution Research** 24 (2017) 12599-12607.

[27] K.Z. Elwakeel, Removal of arsenate from aqueous media by magnetic chitosan resin immobilized with molybdate oxoanions, **International Journal of Environmental Science and Technology** 11 (2014) 1051-1062.

[28] K:Z. Elkaweel, E. Guibal, Arsenic(V) sorption using chitosan/$Cu(OH)_2$ and chitosan/CuO composite sorbents, **Carbohydrate Polymers** 134 (2015) 190-204.

[29] L. Demarchis, M. Minella, R. Nisticò, V. Maurino, C. Minero, D. Vione, Photo-Fenton reaction in the presence of morphologically controlled hematite as iron source, **Journal of Photochemistry and Photobiology A: Chemistry** 307 (2015) 99-107.

[30] F. Cesano, G. Fenoglio, L. Carlos, R. Nisticò, One-step synthesis of magnetic chitosan polymer composite films, **Applied Surface Science** 345 (2015) 175-181.

[31] F. Franzoso, R. Nisticò, F. Cesano, I. Corazzari, F. Turci, D. Scarano, A. Bianco Prevot, G. Magnacca, L. Carlos, D.O. Mártire, Biowaste-derived substances as a tool for obtaining magnet-sensitive materials for environmental applications in wastewater treatments, **Chemical Engineering Journal** 310 (2017) 307-316.

[32] R. Nisticò, Magnetic materials and water treatments for a sustainable future, **Research on Chemical Intermediates**, 2017. https://doi.org/10.1007/s11164-017-3029-x.

[33] R. Nisticò, F. Franzoso, F. Cesano, D. Scarano, G. Magnacca, L. Carlos, M.E. Parolo, Chitosan-derived iron oxide systems for magnetically-guided and efficient water purification processes from polycyclic aromatic hydrocarbons, **ACS Sustainable Chemistry and Engineering** 5 (2017) 793-801.

[34] R. Nisticò, M. Barrasso, G.A. Carrillo Le Roux, M.M. Seckler, W. Sousa, M. Malandrino, G. Magnacca, Biopolymers from composted biowaste as stabilizers for the green synthesis of spherical and homogeneously sized silver nanoparticles for textile application on natural fibers, **ChemPhysChem** 16 (2015) 3902-3909.

[35] S. Hajji, I. Younes, O. Ghorbel-Bellaaj, R. Hajji, M. Rinaudo, M. Nasri, K. Jellouli, Structural differences between chitin and chitosan extracted from three different marine sources, **International Journal of Biological Macromolecules** 65 (2014) 298–306.

[36] F.A. Al Sagheer, M.A. Al-Sughayer, S. Muslim, M.Z. Elsabee, Extraction and characterization of chitin and chitosan from marine sources in Arabian Gulf, **Carbohydrate Polymers** 77 (2009) 410-419.

[37] F.M. Kerton, Y. Liu, K.W. Omari, K. Hawboldt, Green chemistry and the ocean-based biorefinery, **Green Chemistry** 15 (2013) 860-871.

[38] R. Nisticò, M.G. Faga, G. Gautier, G. Magnacca, D. D'Angelo, E. Ciancio, G. Piacenza, R. Lamberti, S. Martorana, Physico-chemical characterization of functionalized polypropylenic fibers for prosthetic applications, **Applied Surface Science** 258 (2012) 7889-7896.

[39] P. Avetta, R. Nisticò, M.G. Faga, D. D'Angelo, E. Aimo Boot, R. Lamberti, S. Martorana, P. Calza, D. Fabbri, G. Magnacca, Hernia-repair prosthetic devices functionalised with chitosan and ciprofloxacin coating: Controlled release and antibacterial activity, **Journal of Materials Chemistry B** 2 (2014) 5287-5294.

[40] R. Crisafully, M.A.L. Milhome, R.M. Cavalcante, E.R. Silveira, D. De Keukeleire, R.F. Nascimento, Removal of some polycyclicaromatic hydrocarbons from petrochemical wastewater using low-cost adsorbents of natural origin, **Bioresource Technology** 99 (2008) 4515-4519.

[41] Y. Li, D. Yuan, M. Dong, Z. Chai, G. Fu, Facile and green synthesis of core-shell structured magnetic chitosan submicrospheres and their surface functionalization, **Langmuir** 29 (2013) 11770-11778.

[42] A.H. Lu, E.L. Salabas, F. Schüth, Magnetic nanoparticles: Synthesis, protection, functionalization, and application, **Angewandte Chemie International Edition** 46 (2007) 1222-1244.

[43] I. Corazzari, R. Nisticò, F. Turci, M.G. Faga, F. Franzoso, S. Tabasso, G. Magnacca, Advanced physico-chemical characterization of chitosan by means of TGA coupled on-line with FTIR and GCMS: Thermal degradation and water adsorption capacity, **Polymer Degradation and Stability** 112 (2015) 1-9.

[44] F. Thomas, J.Y. Bottero, and J.M. Cases. 1989. An experimental study of the adsorption mechanisms of aqueous organic acids on porous aluminas. 1. The porosity of the adsorbent: A determining factor for the adsorption mechanisms. **Colloids and Surfaces** 37: 269-280.

[45] I. Langmuir, The adsorption of gases on plane surfaces of glass, mica and platinum, **Journal of the American Chemical Society** 40 (1918) 1361-1403.

[46] H.M.F. Freundlich, Uber die adsorption in losungen, **Zeitschrift für Physikalische Chemie** 57 (1906) 385-470.

[47] H. Zheng, Y. Wang, Y. Zheng, H. Zhang, S. Liang, M. Long, Equilibrium, kinetic and thermodynamic studies on the sorption of 4-hydroxyphenol on Cr-bentonite, **Chemical Engineering Journal** 143 (2008) 117-123.

[48] J. Safari, L. Javadian, Chitosan decorated Fe_3O_4 nanoparticles as a magnetic catalyst in the synthesis of phenytoin derivatives, **RSC Advances** 4 (2014) 48973-48979.

[49] H. Salehizadeh, E. Hekmatian, M. Sadeghi, K. Kennedy, Synthesis and characterization of core-shell Fe_3O_4-gold-chitosan nanostructure, **Journal of Nanobiotechnology** (2012), 10:3. doi: 10.1186/1477-3155-10-3.

[50] X. Ou, S. Chen, X. Quan, H. Zhao, Photochemical activity and characterization of the complex of humic acids with iron(III), **Journal of Geochemical Exploration** 102 (2009) 49-55.

[51] R.M. Cornell, U. Schwertmann, *The Iron Oxides: Structure, Properties, Reactions, Occurrences and Uses*, Wiley-VCH, Weinheim, Germany, 2003.

[52] X. Sun, C. Zheng, F. Zhang, Y. Yang, G. Wu, A. Yu, N. Guan, Size-controlled synthesis of magnetite (Fe_3O_4) nanoparticles coated with glucose and gluconic acid from a single Fe(III) precursor by a sucrose bifunctional hydrothermal method, **Journal of Physical Chemistry C** 113 (2009) 16002-16008.

[53] D.K. Kim, M. Mikhaylova, Y. Zhang, M. Muhammed, Protective coating of superparamagnetic iron oxide nanoparticles, **Chemistry of Materials** 15 (2003) 1617-1627.

[54] G. Ungureanu, S. Santos, R. Boaventura, C. Botelho, Arsenic and antimony in water and wastewater: Overview of removal techniques with special reference to latest advances in adsorption, **Journal of Environmental Management** 151 (2015) 326–342.

[55] S. Lunge, S. Singh, A Sinha, Magnetic iron oxide (Fe_3O_4) nanoparticles from tea waste for arsenic removal, **Journal of Magnetism and Magnetic Materials** 356 (2014) 21-31.

[56] A. Gupta, V.S. Chauhan, N. Sankararamakrishnan, Preparation and evaluation of iron-chitosan composites for removal of As(III) and As(V) form arsenic contaminated real life groundwater, **Water Research** 43 (2009) 3862-3870.

[57] J. Jonsson, D.M. Shermann, Sorption of As(III) and As(V) to siderite, green rust (fougerite) and magnetite: Implications for arsenic release in anoxic groundwaters, **Chemical Geology** 255 (2008) 173–181.

[58] Y. Yoon, W.K. Park, T.-M. Hwang, D.H. Yoon, W.S. Yang, J.-W. Kang, Comparative evaluation of magnetite-graphene oxide and magnetite-reduced grapheme oxide composite for As(III) and As(V) removal, **Journal of Hazardous Materials** 304 (2015) 196-204.

[59] M. Shimizu, M. Ginder-Vogel, S.J. Parikh, D.L. Sparks, Molecular scale assessment of methylarsenic sorption on aluminum oxide, **Environmental Science and Technology** 44 (2010) 612-617.

[60] N. Can, B. Can Ömür, A. Altındal, Modeling of heavy metal ion adsorption isotherms onto metallophthalocyanine film, **Sensors and Actuators B** 237 (2016) 953-961.

[61] K.Y. Foo, B.H. Hameed. Insights into the modeling of adsorption isotherm systems, **Chemical Engineering Journal** 156 (2010) 2–10.

[62] N.J. Barrow, The description of sorption curves, **European Journal of Soil Science** 59 (2008) 900–910.

[63] D. Mohan, C.U. Pittman Jr., Arsenic removal from water/wastewater using adsorbents-A critical review, **Journal of Hazardous Materials** 142 (2007) 1-53.

[64] W. Yang, N. Zhao, N. Zhang, W. Chen, A.T. Kan, M.B. Tomson, Time-dependent adsorption and resistant desorption of arsenic on magnetite nanoparticles: kinetics and modeling, **Desalination and Water Treatment** 44 (2012) 100–109.

[65] L. Charlet G. Morin, J. Rose, T. Wang, M. Auffan, A. Burinol, A. Fernandez-Martinez, Reactivity at (nano)particle-water interfaces, redox processes, and arsenic transport in the environment, **Comptes Rendus Geoscience** 343 (2011) 123–139.

[66] G. Morin, Y. Wang, G. Ona-Nguema, F. Juillot, G. Calas, N. Menguy, E. Aubry, J.R. Bargar, G.E. Brown Jr., EXAFS and HRTEM evidences for As(III)-containing surface precipitates on nanocrystalline magnetite: implications for As sequestration, **Langmuir** 25 (2009) 9119–9128.

[67] C.-H. Liu, Y.-H. Chuang, T.-Y. Chen, Y. Tian, H. Li, M.-K. Wang, W. Zhang, Mechanism of arsenic adsorption on magnetite nanopartciles from water: Thermodynamic and spectroscopic studies, **Environmental Science and Technology** 49 (2015) 7726–7734.

[68] F.-J. Zhao, Y.-G. Zhu, A.A. Meharg, Methylated arsenic species in rice: Geographical variation, origin, and uptake mechanisms, **Environmental Science and Technology** 47 (2013) 3957-3966.

[69] J.-H. Huang, E. Matzner, Dynamics of organic and inorganic arsenic in the solution phase of an acidic fen in Germany, **Geochimica et Cosmochimica Acta** 70 (2006) 2023–2033.

[70] D. Zhao, Y. Yu, C. Wang, J.P. Chen, Zirconium/PVA modified flat-sheet PVDF membrane as a cost-effective adsorptive and filtration material: A case study on decontamination of organic arsenic in aqueous solutions, **Journal of Colloid and Interface Science** 477 (2016) 191–200.

[71] M. Shimizu, Y. Arai, D.L. Sparks, Multiscale assessment of methylarsenic reactivity in soil: 1. Sorption and desorption on soil, **Environmental Science and Technology** 45 (2011) 4293-4299.

[72] M. Shimizu, Y. Arai, D.L. Sparks, Multiscale assessment of methylarsenic reactivity in soil: 2. Distribution and speciation in soil, **Environmental Science and Technology** 45 (2011) 4300-4306.

[73] Y.-T. Wei, Y.-M. Zheng, J.P. Chen, Uptake of methylated arsenic by a polymeric adsorbent: Process performance and adsorption chemistry, **Water Research** 45 (2011) 2290–2296.

Captions to Figures

Table 1. Comparison of estimated parameters obtained from both Langmuir and Freundlich isotherms.

Figure 1. Physicochemical and magnetic characterization of chitosan-derived (left) and BBS-derived (right) magnet-sensitive materials. Panels A and B: XRD patterns of M0 (blue dotted curve), MC0 (black solid curve), MCP (black dotted curve), MB0 (red solid curve) and MBP (red dotted curve). Magnetite/maghemite crystalline planes reflections are highlighted (colored background). Panels C and D: Absorbance FTIR spectra in the 4000-400 cm^{-1} range relative to M0 (blue dotted curve), MC0 (black solid curve), MCP (black dotted curve), reference chitosan (CHI, blue solid curve), MB0 (red solid curve), MBP (red dotted curve), and reference BBS (BBS, green solid curve). Main peaks are highlighted (colored background). Panels E and F: Magnetization curves evaluation of M0 (blue empty squares), MC0 (black full circles), MCP (black empty circles), MB0 (red triangles), and MBP (red empty triangles).

Figure 2. Adsorption isothermal experiments of both As(V) (A, left) and As(III) (B, right) on MC0 (black circles), MCP (white circles), MB0 (red triangles), and MBP (white triangles). Experimental conditions: [sorbent] = 2000 mg L^{-1}, [As] = 5-300 mg L^{-1}, contact time = 24h. All experiments are performed maintaining constant the temperature (25°C in the dark), the pH (pH = 6.0) and the ionic strength ([KCl] = 0.01M).

Figure 3. Desorption experiments of both As(V) (top) and As(III) (bottom) from MCP (left) and MBP (right). Legend: residual As irreversibly bonded to the sorbent surface (grey), As removed after washing with 0.01M KCl (black) and 0.1M K_2HPO_4 (red). Experimental conditions: [sorbent] = 2000 mg L^{-1}, contact time = 24h, T = 25°C, and pH = 6.0.

Figure 4. Adsorption isothermal experiments of DMA on both MCP (white circles), and MBP (white triangles). Experimental conditions: [sorbent] = 2000 mg L^{-1}, [As] = 5-240 mg L^{-1}, contact time = 24h. All experiments are performed maintaining constant the temperature (25°C in the dark), the pH (pH = 6.0) and the ionic strength ([KCl] = 0.01M).

Figure 5. Desorption experiments of DMA from MCP (A, left) and MBP (B, right). Legend: residual As irreversibly bonded to the sorbent surface (grey), As removed after washing with 0.01M KCl (black) and 0.1M K_2HPO_4 (red). Experimental conditions: [sorbent] = 2000 mg L^{-1}, contact time = 24h, T = 25°C, and pH = 6.0.

Table 1. Comparison of estimated parameters obtained from both Langmuir and Freundlich isotherms.

Sample	Adsorbate	Langmuir model			Freundlich model		
		R^2	q_0	b	R^2	n	K_F
MCP	As(V)	0.879	84.1	2.6	0.950	3.7	30.4
MCP	As(III)	0.970	17.1	0.2	0.920	4.8	6.1
MCP	DMA	0.927	9.0	2.0	0.662	11.1	5.8
MBP	As(V)	0.832	43.9	1.2	0.900	4.8	18.6
MBP	As(III)	0.954	17.2	0.4	0.843	5.7	7.4
MBP	DMA	0.854	17.2	0.1	0.929	3.4	3.9

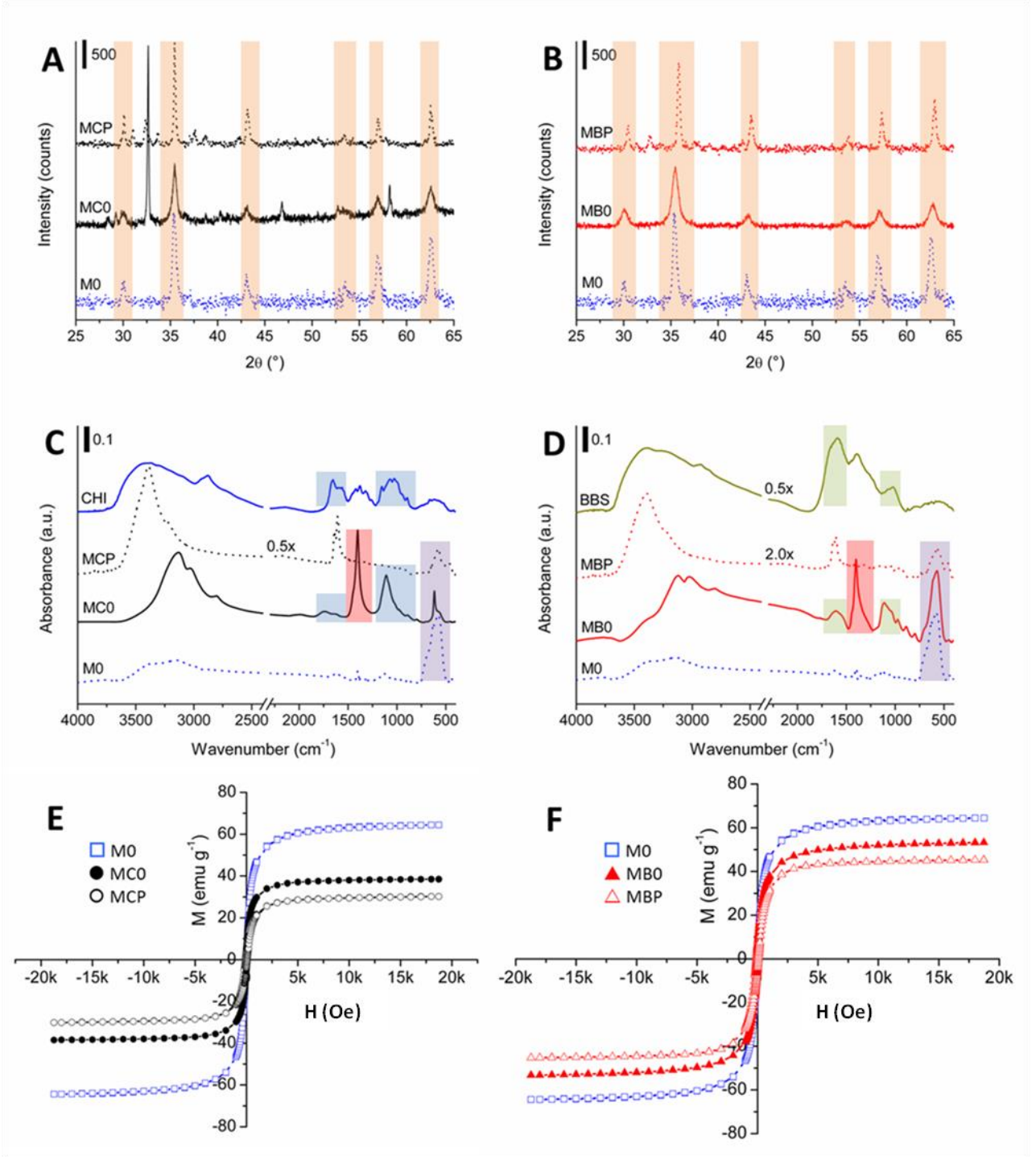

Figure 1. Physicochemical and magnetic characterization of chitosan-derived (left) and BBS-derived (right) magnet-sensitive materials. Panels A and B: XRD patterns of M0 (blue dotted curve), MC0 (black solid curve), MCP (black dotted curve), MB0 (red solid curve) and MBP (red dotted curve). Magnetite/maghemite crystalline planes reflections are highlighted (colored background). Panels C and D: Absorbance FTIR spectra in the 4000-400 cm^{-1} range relative to M0 (blue dotted curve), MC0 (black solid curve), MCP (black dotted curve), reference chitosan (CHI, blue solid curve), MB0 (red solid curve), MBP (red dotted curve), and reference BBS (BBS, green solid curve). Main peaks are highlighted (colored background). Panels E and F: Magnetization

curves evaluation of M0 (blue empty squares), MC0 (black full circles), MCP (black empty circles), MB0 (red triangles), and MBP (red empty triangles).

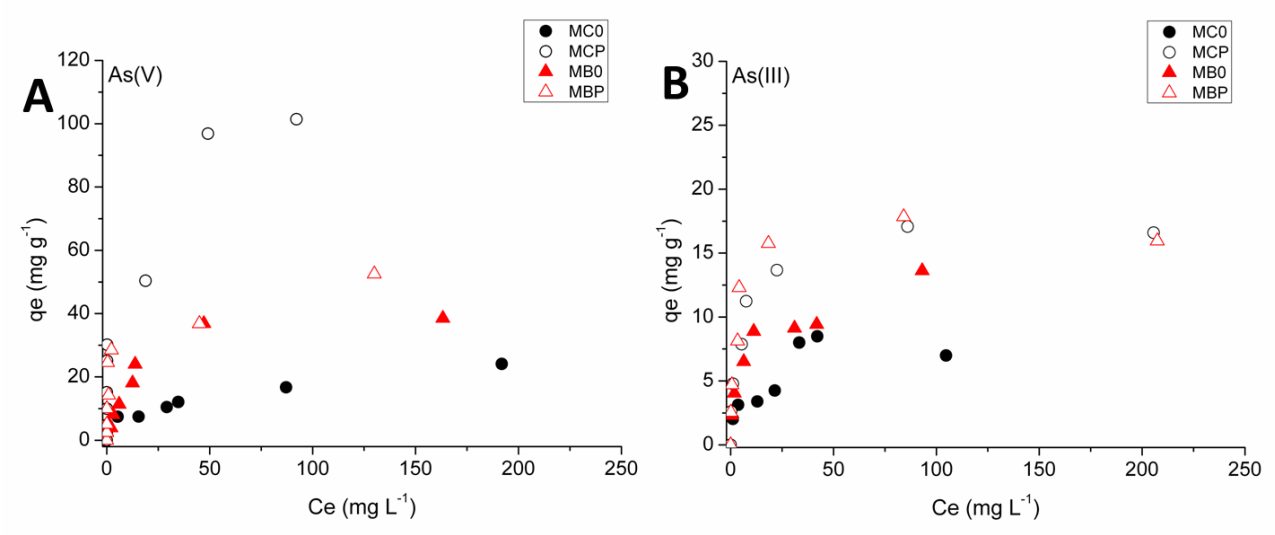

Figure 2. Adsorption isothermal experiments of both As(V) (A, left) and As(III) (B, right) on MC0 (black circles), MCP (white circles), MB0 (red triangles), and MBP (white triangles). Experimental conditions: [sorbent] = 2000 mg L^{-1}, [As] = 5-300 mg L^{-1}, contact time = 24h. All experiments are performed maintaining constant the temperature (25°C in the dark), the pH (pH = 6.0) and the ionic strength ([KCl] = 0.01M).

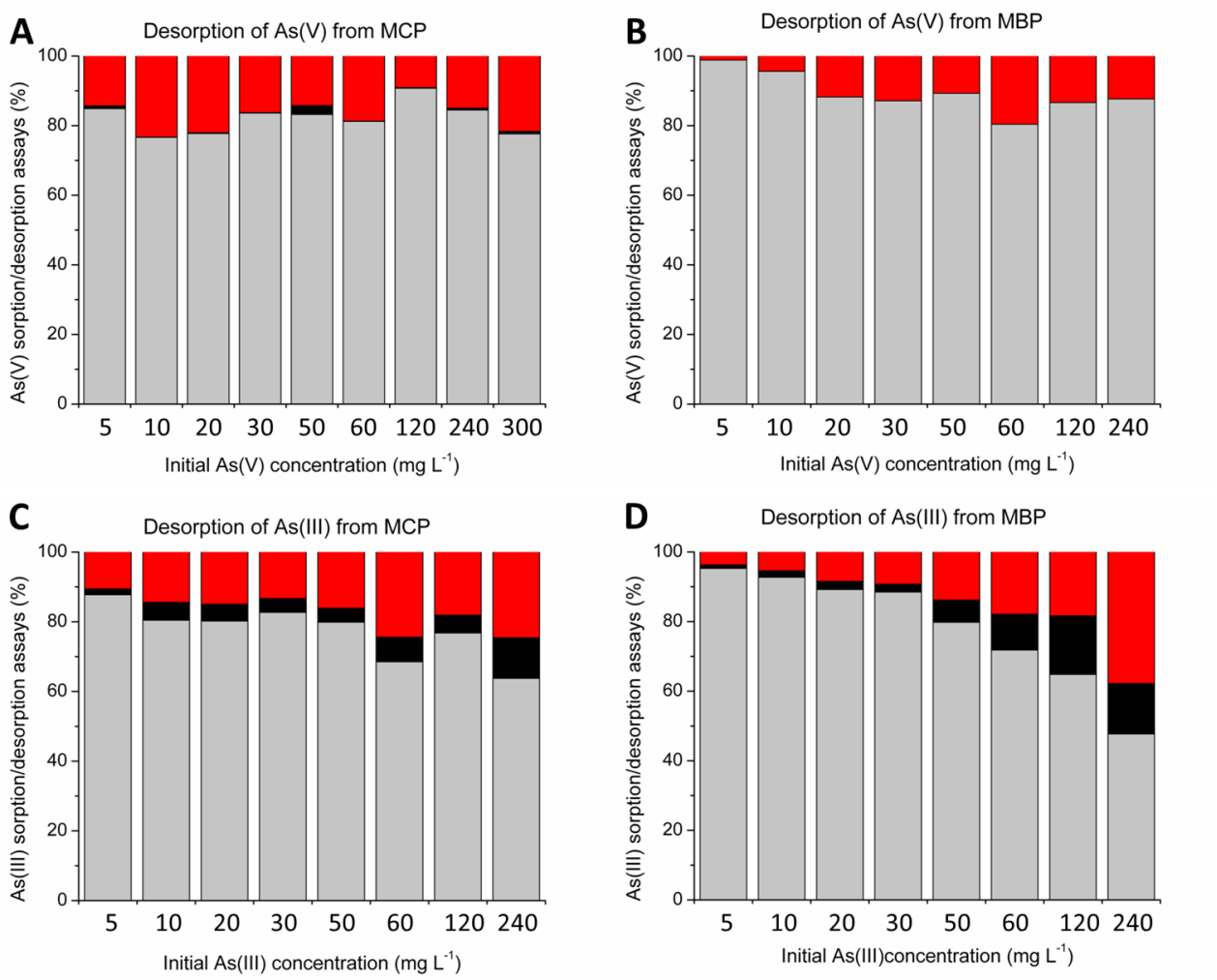

Figure 3. Desorption experiments of both As(V) (top) and As(III) (bottom) from MCP (left) and MBP (right). Legend: residual As irreversibly bonded to the sorbent surface (grey), As removed after washing with 0.01M KCl (black) and 0.1M K_2HPO_4 (red). Experimental conditions: [sorbent] = 2000 mg L^{-1}, contact time = 24h, T = 25°C, and pH = 6.0.

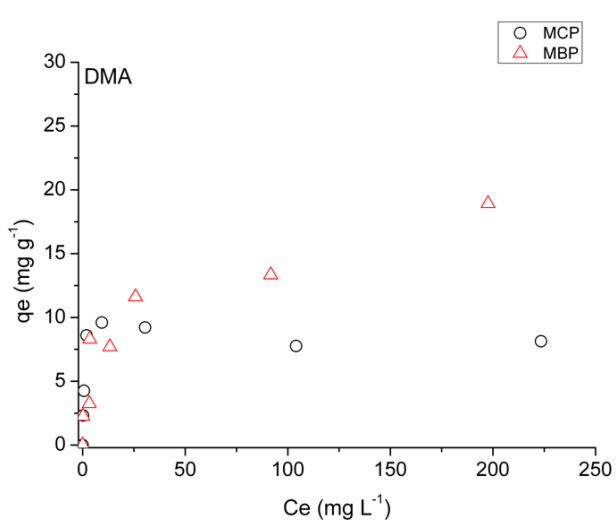

Figure 4. Adsorption isothermal experiments of DMA on both MCP (white circles), and MBP (white triangles). Experimental conditions: [sorbent] = 2000 mg L^{-1}, [As] = 5-240 mg L^{-1}, contact time = 24h. All experiments are performed maintaining constant the temperature (25°C in the dark), the pH (pH = 6.0) and the ionic strength ([KCl] = 0.01M).

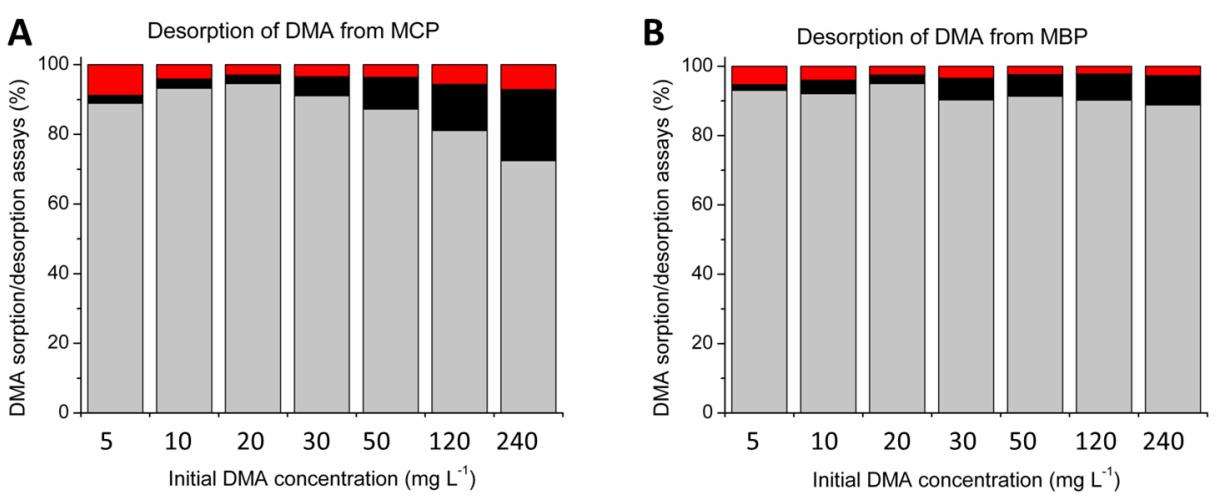

Figure 5. Desorption experiments of DMA from MCP (A, left) and MBP (B, right). Legend: residual As irreversibly bonded to the sorbent surface (grey), As removed after washing with 0.01M KCl (black) and 0.1M K_2HPO_4 (red). Experimental conditions: [sorbent] = 2000 mg L^{-1}, contact time = 24h, T = 25°C, and pH = 6.0.